Semi-Permeable Filters for Interior Region of Interest Dose Reduction in X-Ray Microscopy

Yixing Huang[1], Leonid Mill[1], Robert Stoll[1], Lasse Kling[2,4], Oliver Aust[3], Fabian Wagner[1], Anika Grüneboom[3], Georg Schett[3], Silke Christiansen[2,4,5], Andreas Maier[1]

[1]Pattern Recognition Lab, Friedrich-Alexander-University Erlangen-Nuremberg*
[2]Korrelative Mikroskopie und Materialdaten, Fraunhofer-Institut für Keramische Technologien und Systeme IKTS, Forchheim
[3]Institute of clinical Immunology, University Hospital Erlangen
[4]Institut für Nanotechnologie und korrelative Mikroskopie, Forchheim
[5]Physics Department, Freie Universität Berlin, Berlin
yixing.yh.huang@fau.de

Abstract. In osteoporosis research, the number and size of lacunae in cortical bone tissue are important characteristics of osteoporosis development. In order to reconstruct lacunae well in X-ray microscopy while protecting bone marrow from high-dose damage in in-vivo experiments, semi-permeable X-ray filters are proposed for dose reduction. Compared with an opaque filter, image quality with a semi-permeable filter is improved remarkably. For image reconstruction, both iterative reconstruction with reweighted total variation (wTV) and FDK reconstruction from penalized weighted least-square (PWLS) processed projections can reconstruct lacunae when the transmission rate of the filter is as small as 5%. However, PWLS is superior in computation efficiency.

1 Introduction

In today's aging society, there has been a dramatic increase in the occurrence of osteoporosis and related diseases. Osteoporosis is a "progressive systemic skeletal disease characterized by low bone mass and microarchitectural deterioration of bone tissue, with a consequent increase in bone fragility and susceptibility to fracture", as described by WHO. To investigate the development of osteoporosis and its corresponding treatment, the microanalysis of bone tissue is necessary. In this work, tibial bones from aging mouse models are used, which in general have very fine structures. A mouse tibial bone mainly contains exterior cortical bone tissue and interior bone marrow. The number and size of lacunae in the cortical bone tissue are important characteristics of osteoporosis development. Therefore, the bone tissue region is of interest for osteoporosis research. The bone marrow

* Y. Huang, L. Mill and R. Stoll contributed equally.

consists of hematopoietic cells, marrow adipose tissue and supportive stromal cells, which is vital for the health of mice.

With modern X-ray microscopy (XRM) systems, high resolution images are reconstructed with a voxel size up to 500 nm, which allows the investigation of bone structures in nano-scale in a nondestructive manner [1]. However, such a high resolution reconstruction requires around 2000 projections with acquisition time up to several hours. The large amount of X-ray dose will damage bone marrow [2] and thereby affects the natural osteoporosis development in in-vivo experiments. Therefore, we aim to avoid the high dose exposure to bone marrow while preserving the good image quality of exterior cortical bone tissue.

For dose reduction, collimators are widely used in computed tomography (CT) for region-of-intrest (ROI) imaging. They are typically placed to block exterior X-ray exposure for interior tomography [3]. However, in our application, since the exterior region is of interest, blocking the X-rays for the central bone marrow area leads to insufficient measured data for the exterior area as well, which is an exterior tomography problem [4]. Image reconstruction for exterior tomography is very challenging because of data truncation and missing data. Therefore, semi-permeable collimators, commonly called X-ray filters [5], are proposed for our application. In this work, the image quality using filters of different transmission rates and different reconstruction algorithms is investigated.

2 Materials and Methods

2.1 Filter design

The attenuation of X-rays in a filter follows the Beer-Lambert Law

$$I_c = I_0 e^{-\eta}, \tag{1}$$

where I_0 is the intensity of the incident X-ray without filtration and I_c is the X-ray after filtration. η is the filter attenuation determined by the X-ray energy E, the filter material type (defining the mass attenuation coefficient $\mu_m(E)$ and the density ρ), and the filter thickness l

$$\eta = \mu_m(E) \cdot l \cdot \rho. \tag{2}$$

The mass attenuation coefficient μ_m and the density ρ for different materials are available in the NIST Standard Reference Database 126[1]. We further denote the filter transmission rate by $\alpha = I_c/I_0 = e^{-\eta}$. In order to design a filter with a transmission rate α, the filter thickness needs to be $l = -\ln(\alpha)/(\rho \cdot \mu_m)$. For example, with a photon energy of 40 KeV, aluminum has $\mu_m = 0.5685\,\mathrm{cm}^2/\mathrm{g}$ and $\rho = 2.70\,\mathrm{g/cm}^3$. Thus, an aluminum filter with a transmission rate of 5% requires a thickness of around 2.0 cm.

In a cone-beam XRM system, we denote the source-to-isocenter distance by D_1 and the filter length by L_0. The filter is placed between the X-ray source

[1] https://www.nist.gov/pml/x-ray-mass-attenuation-coefficients

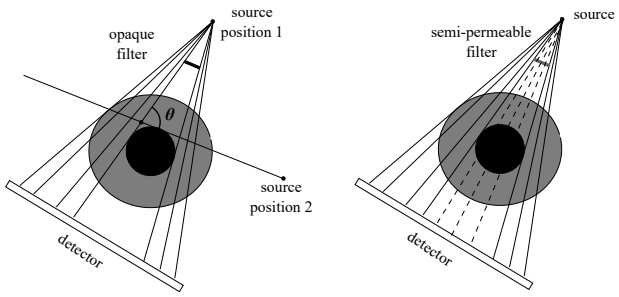

(a) Opaque filter (b) Semi-permeable filter

Fig. 1. Illustration of the effects by an opaque filter and a semi-permeable filter.

and the isocenter with distance D_c to the source. During a 360° scan, a circular area with a diameter of $L = L_0 * D_1/D_c$ is affected by the filter. In practice, the filter length or position can be adjusted according to a preliminary scan using two orthogonal views to align the affected area close to the bone marrow area.

If an opaque filter is applied, i.e. $\alpha = 0$, it changes the angular coverage of X-rays at different locations. Particularly, a point with a distance of d ($d > L$) to the isocenter has an angular range of $\theta = \pi - 2\arctan(L/d)$ for X-ray coverage, as displayed in Fig. 1(a). The closer the points are to the affected area ($d \to L$), the smaller θ is. Therefore, it is very challenging to reconstruct them.

However, with a semi-permeable filter, i.e. $0 < \alpha < 1$, the point still has a full X-ray coverage, but with fewer X-ray photons passing through it (Fig. 1(b)). Due to the reduced number of photons, the X-ray projections contain more quantum (Poisson) noise. According to the Beer-Lambert Law, the detected intensity for the filtered region is as follows

$$I(u, v, \beta) = I_c \cdot e^{-p(u,v,\beta)} = \alpha \cdot I_0 \cdot e^{-p(u,v,\beta)}, \tag{3}$$

where $I(u, v, \beta)$ is the ideal number of X-ray photons at detector pixel (u, v) given the rotation angle β, and $p(u, v, \beta)$ is the total attenuation of the imaged object along the path from the X-ray source at angle β to the detector pixel (u, v). However, due to quantum noise, the actual detected photon number follows a Poisson distribution

$$I_{\text{Poi}} = \mathcal{P}(I(u, v, \beta)), \tag{4}$$

where $\mathcal{P}(\lambda)$ is a Poisson random variable with a mean parameter λ.

2.2 Image reconstruction

In this work, we investigate three algorithms for image reconstruction from filtered data: conventional FDK, iterative reconstruction with reweighted total variation (wTV) regularization [6], and FDK with penalized weighted least-squares (PWLS) [7].

The objective function for wTV with a semi-permeable filter is

$$\min ||\boldsymbol{f}||_{\text{wTV}}, \text{ subject to } ||\boldsymbol{A}_c\boldsymbol{f} - \boldsymbol{p}_c|| < e_c, \text{ and } ||\boldsymbol{A}_n\boldsymbol{f} - \boldsymbol{p}_n|| < e_n. \tag{5}$$

where $||\boldsymbol{f}||_{\mathrm{wTV}}$ is the wTV term defined in [6], $\boldsymbol{p}_{\mathrm{c}}$ and $\boldsymbol{p}_{\mathrm{n}}$ are the filtered and non-filtered projection vectors respectively, $\boldsymbol{A}_{\mathrm{c}}$ and $\boldsymbol{A}_{\mathrm{n}}$ are their corresponding system matrices respectively, and e_{c} and e_{n} are two error tolerance parameters to account for different levels of noise. For image reconstruction with an opaque filter, the data fidelity term $||\boldsymbol{A}_{\mathrm{c}}\boldsymbol{f} - \boldsymbol{p}_{\mathrm{c}}|| < e_{\mathrm{c}}$ is omitted. The above objective function is optimized by alternating simultaneous algebraic reconstruction technique (SART) and the gradient descent of the wTV term [6].

The PWLS objective function in the projection space can be described as [7]

$$\min(\hat{\boldsymbol{p}} - \boldsymbol{p})^{\top} \Lambda^{-1} (\hat{\boldsymbol{p}} - \boldsymbol{p}) + \frac{1}{2} \sum_{i} \sum_{m \in \mathcal{N}_i} (\hat{\boldsymbol{p}}_i - \hat{\boldsymbol{p}}_m)^2, \tag{6}$$

where $\boldsymbol{p}$ is the measured projection vector, $\hat{\boldsymbol{p}}$ is the denoised projection vector, i and m are projection pixel index, and $\mathcal{N}_i$ is the four-nearest neighbor of the i-th pixel. The iterative algorithm in [7] is applied to solve the above objective function. Afterwards, FDK is applied for image reconstruction.

2.3 Experimental Setup

We investigate the effect of different filters using a mouse tibial bone in a simulation study. The projection data are simulated in a XRM system with a source-to-isocenter distance 10 mm and a source-to-detector distance 25 mm. The detector has 2000 × 2000 pixels with a pixel size of 2.0 μm. Poisson noise is simulated considering an initial exposure of 5×10^6 photons at each detector pixel without any filters, i.e. $I_0 = 5 \times 10^6$. In this work, only monoenergetic X-rays are considered. The reconstruction volume has a size of $1024 \times 1024 \times 300$ voxels with an isotropic voxel size of 1.34 μm.

For reconstruction, the parameter e_n is set to 5×10^{-5} for Poisson noise tolerance. The other noise tolerance parameter e_c is set to 5×10^{-5}, 2×10^{-4}, 5×10^{-4}, 10^{-3} and 5×10^{-3} for $\alpha = 1, 25\%, 10\%, 5\%$ and 1%, respectively. For the wTV regularization, 10 iterations of SART + wTV are applied to get the final reconstruction.

3 Results

The reconstruction results of one example slice without any filter or with an opaque filter are displayed in Fig. 3. With the current intensity $I_0 = 5 \times 10^6$, FDK reconstructs the bone very well from non-filtered data. The zoom-in ROI in Fig. 2(b) illustrates that although the image suffers from noise, the major lacunae can still be recognized. For wTV and PWLS, they can reconstruct the bone better with a higher SSIM value of 0.996 and 0.961 respectively, since both of them can suppress Poisson noise. The lacunae in the wTV and PWLS ROIs are also recognized better than those in FDK.

Due to the missing data when using the opaque filter, streak artifacts occur in the cortical bone tissue in Figs. 2(e)-(g). In addition, some regions have apparent

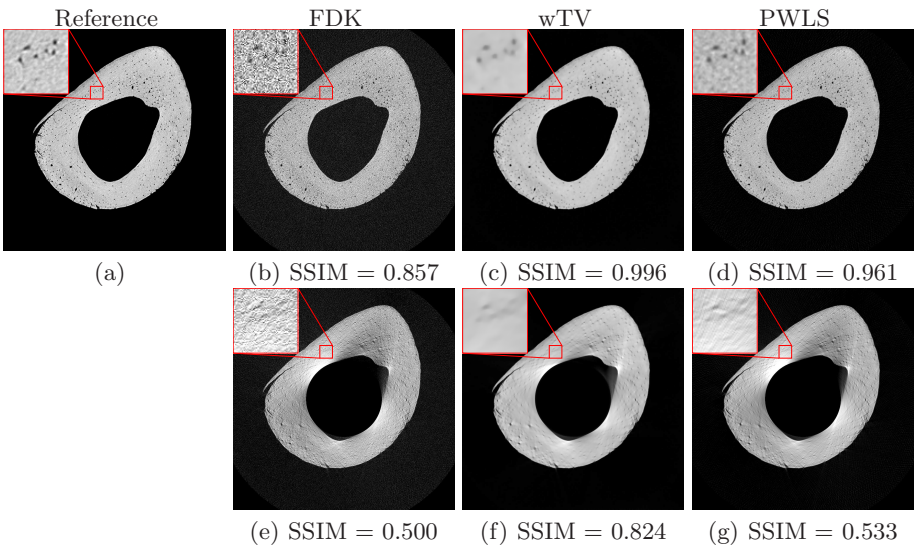

Fig. 2. Reconstruction results of one example slice without any filter (top row) and with an opaque filter (bottom row) using different reconstruction algorithms, window: $[0, 6.25 \times 10^{-5}]/\mu$m. A square ROI containing 6 lacunae is zoomed in.

wrong intensity values, appearing over bright or dark. No matter which algorithm is used, the majority of lacunae are not reconstructed.

The reconstruction results of the example slice with filters of different transmission rates are displayed in Fig. 3. When the transmission rate $\alpha = 0.25\%$, Poisson noise is observed in the FDK reconstruction in Fig. 3(a), especially at the bone marrow area. Consequently, only the locations and sizes of large lacunae can be determined. For $\alpha \leq 10\%$, the lacunae in the zoom-in ROIs are hardly visible in Figs. 3(b)-(d).

For wTV, in Figs. 3(e)-(h) where α varies from 25% to 1%, Poisson noise pattern is not observed in any of the images. Moreover, the lacunae can still be distinguished even though α is as low as 5%. When $\alpha = 1\%$, the lacunae in the ROI lack contrast, although they can be seen to some degree.

PWLS reduces Poisson noise in measured projections. Therefore, in the reconstructed images for α between 25% and 5%, lacunae are observed well. However, for $\alpha = 1\%$, the lacunae in the ROI are only partially visible (Fig. 3(l)).

4 Discussion

With an opaque filter, independently from the reconstruction algorithm, most lacunae are not reconstructed. Using FDK with a transmission rate α smaller than 25%, most lacunae are obscured by Poisson noise. PWLS and wTV are both able to reconstruct lacunae well even when α is as small as 5%. However, PWLS is more efficient than wTV. Therefore, using PWLS with a 5% filter is an optimal option in terms of computation efficiency and image quality.

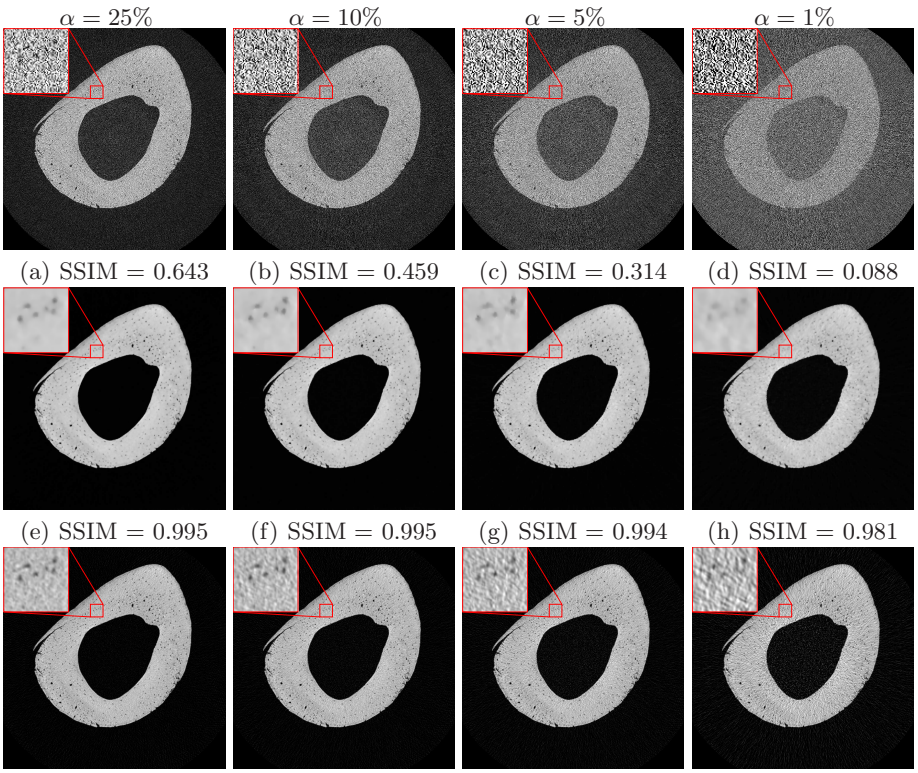

Fig. 3. Reconstruction results of the example slice with filters of different transmission rates, window: $[0,\ 6.25 \times 10^{-5}]/\mu$m. The top, middle and bottom rows are for FDK, wTV and PWLS, respectively.

References

1. Mill L, Kling L, Grüneboom A, et al. Towards In-Vivo X-Ray Nanoscopy: Acquisition Parameters vs. Image Quality. Proc BVM. 2019; p. 251–256.
2. Auvinen A, Bridges J, Dawson K, et al. Health effects of security scanners for passenger screening (based on X-ray technology). SCENIHR. 2012; p. 24.
3. Wang G, Yu H. The meaning of interior tomography. Phys Med Bio. 2013;58(16).
4. Guo Y, Zeng L, Wang C, et al. Image reconstruction model for the exterior problem of computed tomography based on weighted directional total variation. Appl Math Model. 2017;52:358–377.
5. Mail N, Moseley D, Siewerdsen J, et al. The influence of bowtie filtration on cone-beam CT image quality. Med phys. 2009;36(1):22–32.
6. Huang Y, Taubmann O, Huang X, et al. Scale-space anisotropic total variation for limited angle tomography. IEEE Trans Radiat Plasma Med Sci. 2018;2(4):307–314.
7. Wang J, Li T, Lu H, et al. Penalized weighted least-squares approach to sinogram noise reduction and image reconstruction for low-dose X-ray computed tomography. IEEE Trans Med Imaging. 2006;25(10):1272–1283.